

# Discovery of Inhibitors of 4'-Phosphopantetheine Adenylyltransferase (PPAT) To Validate PPAT as a Target for Antibacterial Therapy

Boudewijn L. M. de Jonge,<sup>a</sup> Grant K. Walkup,<sup>a</sup> Sushmita D. Lahiri,<sup>a</sup> Hoan Huynh,<sup>b</sup> Georg Neckermann,<sup>a</sup> Luke Utley,<sup>c\*</sup> Tory J. Nash,<sup>a</sup> Jesse Brock,<sup>a</sup> Maryann San Martin,<sup>a</sup> Amy Kutschke,<sup>a</sup> Michele Johnstone,<sup>a</sup> Valerie Laganas,<sup>a</sup> Laurel Hajec,<sup>a</sup> Rong-Fang Gu,<sup>a</sup> Haihong Ni,<sup>b,\*</sup> Brendan Chen,<sup>b</sup> Kim Hutchings,<sup>b,\*</sup> Elise Holt,<sup>b</sup> David McKinney,<sup>b</sup> Ning Gao,<sup>a</sup> Stephania Livchak,<sup>a</sup> Jason Thresher<sup>a</sup>

Infection Bioscience, AstraZeneca R&D Boston, Waltham, Massachusetts, USA<sup>a</sup>; Infection Chemistry, AstraZeneca R&D Boston, Waltham, Massachusetts, USA<sup>b</sup>; Infection DMPK, AstraZeneca R&D Boston, Waltham, Massachusetts, USA<sup>c</sup>

**Inhibitors of 4'-phosphopantetheine adenylyltransferase (PPAT) were identified through high-throughput screening of the AstraZeneca compound library. One series, cycloalkyl pyrimidines, showed inhibition of PPAT isozymes from several species, with the most potent inhibition of enzymes from Gram-positive species. Mode-of-inhibition studies with *Streptococcus pneumoniae* and *Staphylococcus aureus* PPAT demonstrated representatives of this series to be reversible inhibitors competitive with phosphopantetheine and uncompetitive with ATP, binding to the enzyme-ATP complex. The potency of this series was optimized using structure-based design, and inhibition of cell growth of Gram-positive species was achieved. Mode-of-action studies, using generation of resistant mutants with targeted sequencing as well as constructs that overexpress PPAT, demonstrated that growth suppression was due to inhibition of PPAT. An effect on bacterial burden was demonstrated in mouse lung and thigh infection models, but further optimization of dosing requirements and compound properties is needed before these compounds can be considered for progress into clinical development. These studies validated PPAT as a novel target for antibacterial therapy.**

Bacterial infections remain a significant cause of mortality and morbidity worldwide, in main part due to the emergence of resistance to clinically approved antibacterial drugs (1, 2, 3, 4). As a result, novel drugs are needed to treat infections caused by these resistant isolates (5, 6). Rather than optimizing existing classes of antibacterial agents, an alternative avenue to pursue new drugs is to seek out targets that have not been used previously in antibacterial therapy, as this approach avoids cross-resistance on the compound level as well as the target level. Advancements in genomics, high-throughput screening of compound libraries, and structure-based design have allowed the exploration of many novel targets for antibacterial therapy (7, 8, 9). One of the targets explored was 4'-phosphopantetheine adenylyltransferase (PPAT) (8, 10). Validation of this target for antibacterial therapy remained uncertain, however, since none of the efforts using this target resulted in inhibitors that suppressed bacterial growth (8, 10, 11).

PPAT, encoded by the gene *coaD*, is involved in the biosynthesis of coenzyme A (CoA), a cofactor that functions as an acyl group carrier in a number of central biochemical transformations, such as the tricarboxylic acid (TCA) cycle and fatty acid metabolism (12, 13, 14). It forms a hexamer and catalyzes (in the biological forward direction) the reversible transfer of the adenylyl group of ATP to 4'-phosphopantetheine, yielding dephospho-coenzyme A and inorganic pyrophosphate (Fig. 1) (15, 16). PPAT was shown to be essential for growth through genetic knockout experiments (17). It is present with high sequence conservation in most bacteria (18). Since bacterial PPAT has low sequence homology with human PPAT, identification of selective, broad-spectrum bacterial PPAT inhibitors appears to be feasible (18, 19, 20). To that end, a campaign of high-throughput screening with the AstraZeneca corporate library was initiated using *Streptococcus mutans* PPAT. Several hits were identified, but only one series showed potential for broad-spectrum PPAT inhibition. This series was optimized and yielded analogs that suppress growth *in vitro* and in animal effi-

cacy models through inhibition of PPAT, validating for the first time PPAT as a novel target for antibacterial therapy.

## MATERIALS AND METHODS

**Reagents and compounds.** All chemicals were from Sigma-Aldrich unless otherwise specified. 4'-Phosphopantetheine, obtained from Syncom (Groningen, Netherlands), was prepared according to a published method (21). Compounds used in this study (Fig. 2) were synthesized *in-house* (see the supplemental material).

**Bacterial strains and genetic constructs.** Strains, plasmids, and oligonucleotides used in this study are listed in Table 1. Overexpression of *Streptococcus pneumoniae coaD* in *S. pneumoniae* was achieved by driving expression from the *galU* promoter (22).

**Measurement of cellular activity.** MICs were measured according to CLSI guidelines (23). As trailing was observed with some strains, MICs were defined as the lowest concentration that inhibited >80% of cell growth. MIC<sub>90s</sub> were determined on large panels of clinical strains isolated from various geographic locations with different resistance genotypes and phenotypes and were defined as the lowest concentrations that inhibited growth of ≥90% of the strains.

Inhibition of a human lung carcinoma cell line, A549, was measured by using the CellTiter 96 Aqueous One Solution cell proliferation assay

Received 30 July 2013 Returned for modification 18 August 2013

Accepted 13 September 2013

Published ahead of print 16 September 2013

Address correspondence to Boudewijn L. M. de Jonge, boudewijn.dejonge@astrazeneca.com.

\* Present address: Luke Utley, Agios Pharmaceuticals, Cambridge, Massachusetts, USA; Haihong Ni, BioDuro, Beijing, China; Kim Hutchings, Department of Medicinal Chemistry, College of Pharmacy, University of Michigan, Ann Arbor, Michigan, USA.

Supplemental material for this article may be found at <http://dx.doi.org/10.1128/AAC.01661-13>.

Copyright © 2013, American Society for Microbiology. All Rights Reserved.

doi:10.1128/AAC.01661-13

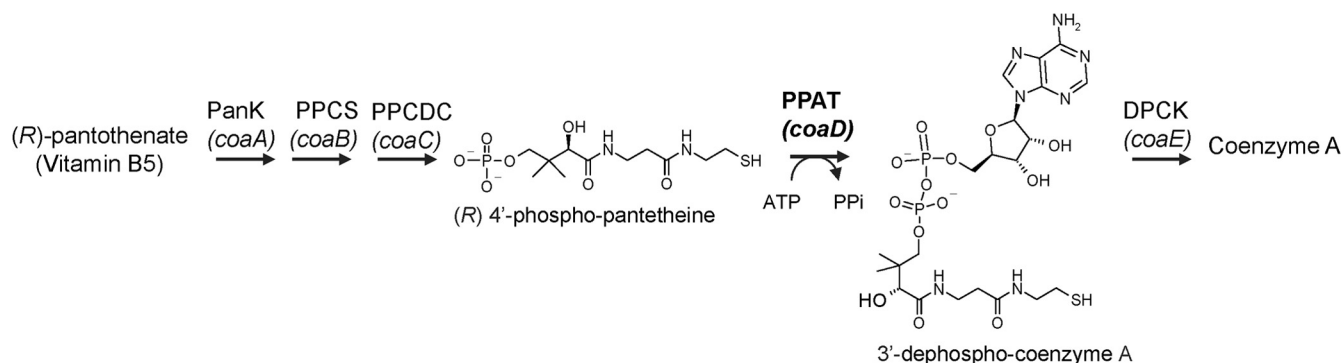


FIG 1 Pathway of CoA biosynthesis and reaction of PPAT.

with MTS [3-(4,5-dimethylthiazol-2-yl)-5-(3-carboxymethoxyphenyl)-2-(4-sulfophenyl)-2H-tetrazolium, inner salt] from Promega Corp. (Madison, WI). A549 cells were grown at 37°C under 5% CO<sub>2</sub> conditions in RPMI 1640 medium supplemented with 10% fetal bovine serum and 1 mM glutamine (Invitrogen, Carlsbad, CA) for 72 h. Cytotoxicity was quantified by determining the lowest compound concentration at which transmission was increased by 50%.

Cidalities of compounds were measured with killing kinetic assays (24) using *Staphylococcus aureus* ARC516 and a LytA<sup>-</sup> strain for *S. pneumoniae* (25).

Spontaneous resistance frequencies for *S. aureus* ARC516 and *S. pneumoniae* D39 were measured by plating in triplicate high inocula of cells on compound-containing plates at up to 8× MIC. Plates were incubated at 37°C, and colonies were counted after 48 h. Spontaneous resistance frequencies were calculated as the ratios of average CFU in the presence and absence of compound.

**Cloning and production of bacterial and human PPAT.** PPAT from the different organisms was cloned and overexpressed in *Escherichia coli* and purified through column chromatography (see the supplemental material). Final proteins were determined to be ≥95% pure by SDS gel electrophoresis, except for the *S. aureus* isozyme, which was obtained at ≥90% purity.

**PPAT biochemical inhibition.** Values for 50% inhibitory concentrations (IC<sub>50</sub>s) in activity against *Streptococcus mutans*, *E. coli*, and *Haemophilus influenzae* PPAT were measured in the reverse direction. The *S. mutans* isozyme was assayed in the reverse direction because a sensitive and balanced (26) high-throughput screening (HTS) assay could be formatted that way at acceptable cost. Assays for *E. coli* and *H. influenzae* enzymes were assayed in the reverse direction to maintain consistency of analysis for the Gram-negative isozymes and to avoid issues arising from the 4'-phosphopantetheine substrate inhibition observed for *H. influen-*

*zae*. Detection of ATP formation was measured either through a hexokinase/glucose-6-phosphate dehydrogenase coupling system analogous to that reported previously for *E. coli* PPAT (16) (*S. mutans* PPAT) or through the ATPlite detection solution system (PerkinElmer) (*E. coli* and *H. influenzae* PPAT). Levels of inhibitory activity of compounds against *S. pneumoniae*, *S. aureus*, and *Homo sapiens* PPAT were measured in the forward direction. For *S. aureus* and *H. sapiens*, formation of pyrophosphate was measured (after conversion to orthophosphate) using a malachite green molybdate solution, prepared as previously described (27). For *S. pneumoniae* PPAT, formation of dephospho-coenzyme A was measured through mass spectrometry analysis. (For experimental details on each of the assays, see the supplemental material.)

***S. aureus* and *S. pneumoniae* PPAT mechanism of inhibition.** Reactions were conducted in quadruplicate at room temperature in buffer containing 50 mM MOPS (morpholinepropanesulfonic acid)-NaOH (pH 7.0), 8 mM MgCl<sub>2</sub>, 1 mM dithiothreitol (DTT), 75 mM NaCl, 0.5 mM EDTA, 0.01% (wt/vol) Brij 35, 0.4 U/ml yeast inorganic pyrophosphatase (Roche), and either 4 nM *S. aureus* or 3 nM *S. pneumoniae* PPAT (calculated as monomers). A matrix of final ATP and 4'-phosphopantetheine concentrations was studied with 2-fold dilutions of each substrate; ATP was adjusted from 1,000 μM to 15.6 μM in both studies. For *S. aureus*, the 4'-phosphopantetheine concentration was adjusted between 150 μM and 2.3 μM and the inhibitor was used at concentrations of 8.1, 2.7, 0.9, 0.3, 0.1, and 0 μM. For *S. pneumoniae*, the 4'-phosphopantetheine concentration was adjusted with doubling dilutions between 800 μM and 50 μM, and the inhibitor was tested at 150, 83, 47, 26, 15, and 0 nM. Reactions were performed in untreated clear polystyrene 384-well plates (Costar) in a 30-μl volume with a 45-μl malachite green molybdate solution quench. Quenched reactions were allowed to incubate for 5 min, and then absorbance at 650 nm was read on a Spectramax plate reader (Molecular Devices). Detection standard curves were made between 0 and 30 μM phos-

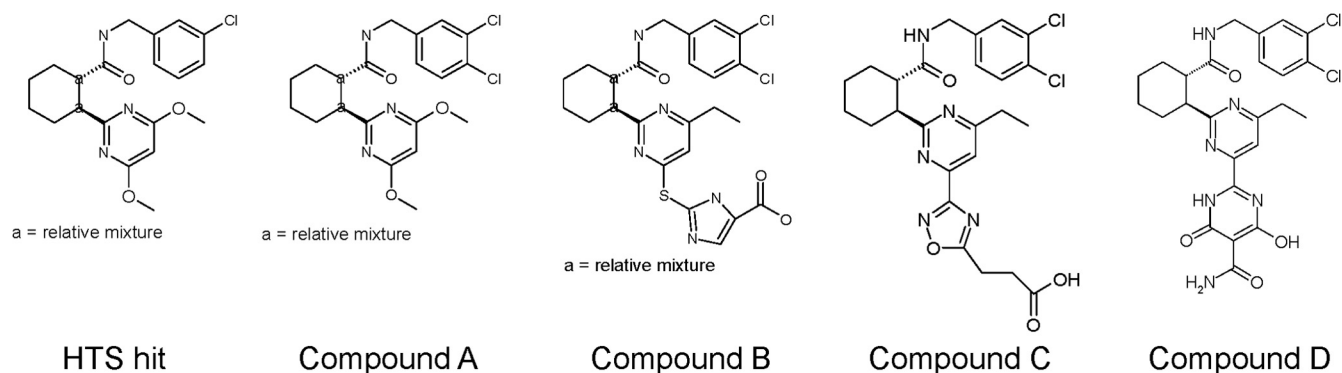


FIG 2 Structures of compounds used in this study.

TABLE 1 Strains, plasmids, and oligonucleotides used in this study

Strain, plasmid, or oligonucleotide	Description	Source or reference
<b>Strains</b>		
<i>E. coli</i> BL21(DE3)	<i>E. coli</i> strain used for protein overexpression	EMD Chemicals
<i>E. coli</i> BL21 pLysS(DE3)	<i>E. coli</i> strain used for protein overexpression with pET23a- <i>Spn CoaD</i>	EMD Chemicals
<i>S. mutans</i> UAB159	Source for <i>coaD</i> of species	ATCC
<i>S. aureus</i> RN4220	Source for <i>coaD</i> of species	22
<i>S. pneumoniae</i> R6	Source for <i>coaD</i> of species	22
<i>H. influenzae</i> Rd (KW20)	Source for <i>coaD</i> of species	22
<i>E. coli</i> MG1655 (K-12)	Source for <i>coaD</i> of species	22
<i>S. pneumoniae</i> D39	Used in susceptibility testing	22
<i>S. pneumoniae</i> ATCC 10813	Clinical isolate used in <i>in vivo</i> studies	ATCC
<i>S. pyogenes</i> ARC838	Clinical isolate used in susceptibility testing	AZ culture collection <sup>a</sup>
<i>S. aureus</i> ARC516	Clinical isolate used in susceptibility testing and <i>in vivo</i> studies	AZ culture collection
<i>E. faecium</i> ARC521	Used in susceptibility testing	AZ culture collection
<i>H. influenzae</i> ATCC 51907	Used in susceptibility testing	ATCC
<i>E. coli</i> W3110	<i>E. coli</i> W3110 <i>tolC</i> gene knockout, used in susceptibility testing	AZ culture collection
<i>E. coli</i> ARC534	Clinical isolate used in susceptibility testing	AZ culture collection
<i>C. albicans</i> ARC527	Clinical isolate used in susceptibility testing	AZ culture collection
<b>Plasmids</b>		
pET23a	General overexpression plasmid	EMD Chemicals
pET30a	General overexpression plasmid	EMD Chemicals
pCR4-TOPO	Subcloning plasmid	Invitrogen
pET30a- <i>Eco coaD</i>	Expression plasmid for <i>E. coli</i> PPAT	This study
pET30a- <i>Hinf coaD</i>	Expression plasmid for <i>H. influenzae</i> PPAT	This study
pET30a- <i>Hsap coaDE</i>	Expression plasmid for <i>H. sapiens</i> PPAT	This study
pET30a- <i>Sau coaD</i>	Expression plasmid for <i>S. aureus</i> PPAT	This study
pET30a- <i>Smu coaD</i>	Expression plasmid for <i>S. mutans</i> PPAT	This study
pET23a- <i>Spn coaD</i>	Expression plasmid for <i>S. pneumoniae</i> PPAT	This study
pBA467- <i>Spn coaD</i>	Plasmid to construct overexpression of PPAT in <i>S. pneumoniae</i>	This study
<b>Oligonucleotides</b>		
<i>Eco coaD</i> F	5'-GACTCATATGCAAAAACGGGCGATTTA-3' (NdeI site underlined)	This study
<i>Eco coaD</i> R	5'-GTCAGTCGACCTACGCTAACTTCGCCATCA-3' (SalI site underlined)	This study
<i>Eco coaD</i> mutF	5'-GAAATGCAGCTGGCGCACATGAATCGCCACTTAATGCCGG-3'	This study
<i>Eco coaD</i> mutR	5'-CCGGCATTAAAGTGGCGATTTCATGTGCGCCAGCTGCATTTC-3'	This study
<i>Hinf coaD</i> F	5'-GCTACATATGACGAGCGTGATTTATCC-3' (NdeI site underlined)	This study
<i>Hinf coaD</i> R	5'-GCTAGTCGACTCATCGTGCTTTAACGCAT-3' (SalI site underlined)	This study
<i>Hsap coaDE</i> F	5'-CACCATGGCCGTATTCGGTCCGGTCTCC-3' (NcoI site underlined)	This study
<i>Hsap coaDE</i> R	5'-ACGTGTCGACTCAGTCGAGGGCCGTGATGAGTCTTGG-3' (SalI site underlined)	This study
<i>Sau coaD</i> F	5'-ACGTCATATGGAACATACAATAGCGGTC-3' (NdeI site underlined)	This study
<i>Sau coaD</i> R	5'-ACGTGTCGACTTAACTTAAATTTCTTCTTCAATGCC-3' (SalI site underlined)	This study
<i>Smu coaD</i> F	5'-GACTCATATGTCAGATAGAATTGGACTC-3' (NdeI site underlined)	This study
<i>Smu coaD</i> R	5'-GATCGTCGACTTAAATTTTTGTTTGTTC-3' (SalI site underlined)	This study
<i>Spn coaD</i> F	5'-ACGTCATATGTCAGATAAGATTGGCTTATTC-3' (NdeI site underlined)	This study
<i>Spn coaD</i> R	5'-ACGTGTCGACCTAATCTTTTTTTCATTTCTTATTTCC-3' (SalI site underlined)	This study

<sup>a</sup> AZ, AstraZeneca R&D Boston.

phate under both low- and high-ATP and -4'-phosphopantetheine conditions to confirm the linearity of the detection system under all assay conditions. Initial rates were calculated from reactions of 0, 10, 20, 30, and 40 min. Rates are expressed as nM pyrophosphate product min<sup>-1</sup> per nM enzyme (calculated as a monomer) for units of min<sup>-1</sup>. Initial rate data were fitted by nonlinear least-squares regression to equations in Grafit 5.0.13 (Erithacus Software). Models for a sequential mechanism of substrate binding were fitted, allowing inhibitor to bind to free enzyme and/or ATP-enzyme complex (see equation 1 below). Here, [A], [B], and [I] are the concentrations of the substrates and inhibitor,  $K_{ma}$  and  $K_{mb}$  are the Michaelis constants for substrates A and B, and  $K_{ia}$ ,  $K_{i1}$ , and  $K_{i2}$  are the dissociation constants ( $K_{dS}$ ) for substrate A from complex EA, inhibitor I from complex EI, and inhibitor I from complex EAI, respectively, as indicated in equation 1:

$$v = \frac{V_{\max}[A][B]}{(K_{ia}K_{mb} + K_{ma}[B])\left(1 + \frac{[I]}{K_{i1}}\right) + (K_{mb}[A])\left(1 + \frac{[I]}{K_{i2}}\right) + [A][B]}$$

**Isothermal titration calorimetry.** Measurements were made with a VP-ITC instrument (Microcal/GE Healthcare, Piscataway, NJ). Solutions of PPAT (generally less than 2 ml) were dialyzed against 2 liters of 50 mM MOPS-NaOH (pH 7.0), 75 mM NaCl, 8 mM MgCl<sub>2</sub>, and 1 mM Tris(2-carboxyethyl)phosphine hydrochloride overnight at 4°C. Titrations were conducted at 25°C. PPAT protein was placed in the instrument cell at a concentration of 60 μM (calculated as a monomer), and compound B was injected at a concentration of 400 μM. Data were analyzed using the software provided by the manufacturer (Origin) and were fitted to both single-site and two-site binding models.

**Measurement of physical chemical and pharmacokinetic (PK) properties.** LogD, plasma protein binding, equilibrium solubility, and clearance in rats for compounds were measured as described before (28).

**X-ray crystallography studies.** Initial crystallization conditions were obtained using sparse matrix crystallization screens (29). The best crystals were grown from 14% to 19% polyethylene glycol 3350 (PEG 3350)–200 mM ammonium sulfate–0.1 M propionic acid cacodylate Bis-tris propane buffer (pH 7.5) (Molecular Dimensions) at 20°C by using the vapor diffusion sitting drop method with a drop size of 2.5  $\mu$ l protein and a 2.5- $\mu$ l reservoir. To obtain an inhibitor-complexed PPAT structure, a 2 mM final concentration of the inhibitor was included in the protein buffer. The crystals grew in 5 to 7 days and were cryoprotected with Paratone-N and flash-frozen in liquid nitrogen prior to data collection. Data for the inhibitor protein cocomplex were collected at Structural GenomiX in Advanced Photon Source. Data processing was done with MOSFLM and scaled with Scala (CCP4 suite). The autoBUSTER software suite (30) was used to index, integrate, and scale the data. Crystallographic refinement was performed using REFMAC, and model building and placement of water molecules was done using COOT (31). The final model quality was assessed using PROCHECK (32). Structural analysis and figures were prepared using Pymol.

**In vivo efficacy studies.** Activity of compounds was assessed in immunocompetent mouse lung and thigh infection models (22, 28). All animal studies were approved by the Institutional Animal Care and Use Committee of AstraZeneca and were conducted in accordance with the guidelines of the American Association for Accreditation of Laboratory Animal Care. Pathogen-free, female CD1 mice, each weighing ca. 20 g (Charles River Laboratories), received oral administrations of aminobenzotriazole (ABT) at 50 mg/kg of body weight 2 h prior and 10 h postinfection to inhibit cytochrome P450 (CYP450) activity (33).

Infection in the lung was established by intratracheal inoculation of *S. pneumoniae* ATCC 10813 ( $1 \times 10^6$  CFU/mouse) (34). Therapy with compounds C and D (Fig. 1) was started 2 h postinfection. Groups of 10 mice each were exposed to 100 mg/kg twice daily (b.i.d.) or four times daily (q.i.d.) every 4 h (q4h). Pyrrolamide compound 26 (35) was dosed orally at 80 mg/kg b.i.d./q12h as a positive control. Control mice received vehicles 15% SBEbCD (Captisol) for compound C and 10% 2-pyrrolidone–0.18% polyvinylpyrrolidone-K30–0.225 M SDS for compound D q.i.d./q4h. All treatments were administered intraperitoneally in a volume of 0.2 ml, and 24 h after the start of compound exposure, mice were euthanized and CFU/lung were determined.

Thigh infections were established with administration of *S. aureus* ARC516 postlaterally into the right thigh muscle to achieve a target starting inoculum of  $1 \times 10^6$  CFU/thigh. Therapy with compound C was administered intraperitoneally starting 2 h after infection, and groups of 10 mice each were exposed to 100 mg/kg twice daily (b.i.d.) or four times daily (q.i.d.) every 4 h (q4h). Linezolid was administered at 160 mg/kg orally once as a positive control, whereas control mice received 15% Captisol (vehicle for compound C) q.i.d./q4h. Mice were euthanized 24 h after the start of treatment, and thighs were homogenized for CFU determinations.

**Protein structure accession numbers.** Coordinates and structure factors have been deposited in the Protein Data Bank under accession numbers 4NAT, 4NAH, and 4NAU.

## RESULTS

**Identification of PPAT inhibitors.** A high-throughput screen of the AstraZeneca compound library with *S. mutans* PPAT identified a dimethoxypyrimidine as an inhibitor. In addition to potent activity against PPAT from *S. mutans* ( $IC_{50} < 100$  nM), this HTS hit (Fig. 2) also showed activity against PPAT isozymes of other species (Table 2), indicating a potential to achieve inhibition of PPAT isozymes of both Gram-positive and Gram-negative species with this series. A medicinal chemistry program was initiated to improve the potency of the compounds against PPAT isozymes.

TABLE 2 Activity for compounds<sup>a</sup>

Parameter	Value for compound:				
	HTS hit	A	B	C	D
<b>Biochemical activity</b>					
<i>S. mutans</i> $IC_{50}$ (nM)	98	ND	ND	ND	2.6
<i>S. pneumoniae</i> $IC_{50}$ (nM)	205	ND	40	0.13	0.065
<i>S. aureus</i> $IC_{50}$ (nM)	7,300	330	490	0.41	0.87
<i>H. influenzae</i> $IC_{50}$ (nM)	8,800	860	9,500	740	120
<i>E. coli</i> $IC_{50}$ (nM)	ND	ND	4,800	330	110
<i>H. sapiens</i> $IC_{50}$ (nM)	ND	>5,000	ND	>200,000	24,000
<b>Cellular activity</b>					
<i>S. pneumoniae</i> MIC ( $\mu$ g/ml)	>64	>64	>64	2	0.03
<i>S. pyogenes</i> MIC ( $\mu$ g/ml)	ND	ND	ND	1	2
<i>S. aureus</i> MIC ( $\mu$ g/ml)	>64	>64	>64	1	0.12
<i>E. faecium</i> ( $\mu$ g/ml)	ND	ND	ND	64	2
<i>H. influenzae</i> MIC ( $\mu$ g/ml)	>64	>64	>64	>64	>64
<i>E. coli</i> MIC ( $\mu$ g/ml)	ND	ND	ND	>64	>64
<i>E. coli</i> MIC ( $\mu$ g/ml) efflux-compromised	>64	>64	>64	>64	>64
<i>C. albicans</i> MIC ( $\mu$ g/ml)	>64	>64	>64	>64	>64
A549 human cell line MIC ( $\mu$ g/ml)	ND	ND	ND	>64	32
<b>Mode of action</b>					
MIC for <i>S. pneumoniae</i> ( $\mu$ g/ml)	ND	ND	ND	1	0.03
MIC for <i>S. pneumoniae</i> ( $\mu$ g/ml) PPAT-overexpressing construct	ND	ND	ND	8	0.25
<b>Other</b>					
LogD	>3	>3	0.69	0.68	2.4
Solubility ( $\mu$ M)	8	<1	850	>1000	73
Human protein binding— $f_u$ (%)	4.6	0.3	1.5	2.0	4.2
Mouse protein binding— $f_u$ (%)	ND	ND	ND	13	11
Rat CL (ml/min/kg)	ND	ND	ND	96	23

<sup>a</sup> For structures, see Fig. 1. ND, not determined;  $f_u$ , fraction unbound.

This program was guided by structure-based design based on cocrystal structures that were obtained with PPAT and dimethoxypyrimidine analogues.

**Optimization of PPAT inhibitors.** Cocrystal structures obtained with PPAT from *S. mutans*, *H. influenzae*, and *S. aureus* showed analogues to be bound in the phosphopantetheine site, in a pocket formed between two monomers. This is exemplified for *S. aureus* PPAT through the comparative overlay of a cocrystal structure of compound A with known substrate-bound structures (36) (Fig. 3A). Polar and hydrophobic interactions were observed between compound and enzyme (Fig. 3B). Hydrogen bonds were observed with the side chains of residues Glu135, Asn107, and Tyr99, and the dichlorophenyl and cyclohexyl moieties of the compound were stabilized by van der Waals interactions with Leu75, Leu38, Met106, Leu103, and Ile87. The cocrystal structure with compound A, obtained early on in the program, indicated room for expansion from the pyrimidine ring toward residues in the ATP-binding pocket and opportunities to establish interactions with residues from the neighboring substrate recognition

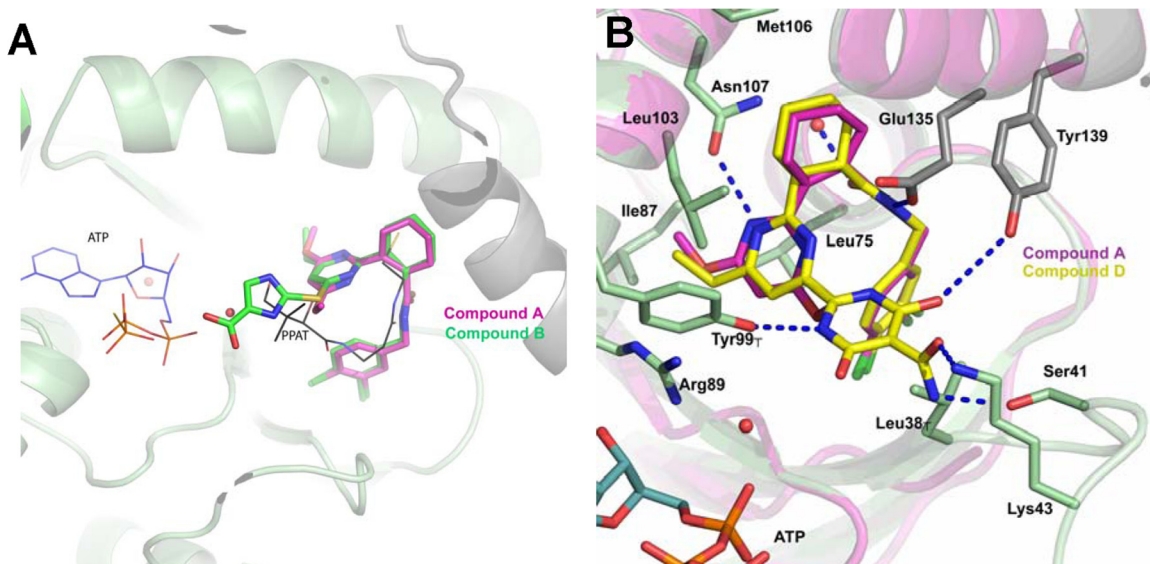


**FIG 3** Cocystal structures of the inhibitors in *S. aureus* PPAT. (A) Structure with compounds A and B overlaid on the ATP- and phosphopantetheine-bound structures of *E. faecalis* PPAT (3ND6 and 3ND7). The image represents the crystal structure of PPAT from *E. faecalis* in the ligand-unbound state and in complex with ATP and pantetheine (36). The compounds bound to the *S. aureus* structure are depicted in the form of a stick model, while substrates ATP (blue) and 4'-phosphopantetheine (black) are shown in a line diagram. The *S. aureus* protein backbones of the two monomers are depicted in green and gray cartoons, respectively. (B) View of the interaction in the binding pocket to compounds A and D showing additional interactions resulting in improved potency. Residues with close interactions are depicted in the form of a stick diagram with the primary monomer colored in green and the adjacent monomer colored in gray. Compound A is shown in pink and compound D is drawn as yellow sticks, while the ATP is shown in cyan. The protein backbone for compound A cocomplex is depicted in pink, while that of compound D is depicted in green and gray.

loop (Ser 41 and Lys43) to improve potency in the series. On the other hand, few improvements in potency could be envisaged with the other rings, as the tight hydrophobic pockets surrounding these groups do not allow for enhanced interactions. Analogues with substitutions on the pyrimidine ring, designed to reach toward the ATP-binding pocket, were synthesized and showed, as expected, potent inhibition of Gram-positive isozymes, with  $IC_{50}$ s in the picomolar range (Table 2, compounds C and D). A cocystal structure of compound D showed that potency was gained through additional interactions with Ser41, Tyr139, and Lys43 (Fig. 3B). As expected, no significant potency enhancements were achieved through modifications on the benzyl and cyclohexyl rings, except for an additional chloro substitution on the benzyl ring (Table 2; compare HTS hit with compound A). Whereas potency improvements were made against all bacterial isozymes, the improvements were more substantial against Gram-positive isozymes (Table 2).

**Mode-of-inhibition studies.** Steady-state inhibition by compound B of the PPAT enzymes from *S. aureus* and *S. pneumoniae* was studied in the forward reaction direction using a matrix of ATP, 4'-phosphopantetheine, and inhibitor concentrations. Initial inspection of reciprocal plots clearly indicated that the enzyme mechanism proceeds through a ternary complex (37), which is consistent with earlier kinetic and structural studies on the *E. coli* enzyme (16, 38, 39). For the *S. aureus* enzyme, the kinetics are complex, with significant substrate inhibition observed for both ATP and 4'-phosphopantetheine substrates (see Fig. S1 in the supplemental material). In contrast, no signs of substrate inhibition were observed for *S. pneumoniae*.

Attempts to fit the *S. aureus* data via nonlinear least-squares methods to common models incorporating substrate inhibition

(40) produced only results with significant deviations between the data and fits, so  $K_i$  for the inhibitor with this enzyme is not reported. However, reciprocal plot analysis clearly demonstrated competitive behavior with respect to 4'-phosphopantetheine and a mixed inhibition profile relative to ATP (Fig. 4).

Analysis of *S. pneumoniae* inhibition data were consistent with inhibitor being competitive with 4'-phosphopantetheine and uncompetitive with ATP (Fig. 5). The inhibition data were fitted to equation 1 via nonlinear least-squares analysis, and parameters from this model are summarized in Table 3. The more potent inhibitor binding mode ( $K_{i2} = 12.2 \pm 0.4$  nM) was for the inhibitor binding to the enzyme-ATP complex. In addition, a weaker inhibitor binding mode ( $K_{i1} = 0.29 \pm 0.05$   $\mu$ M) was identified for inhibitor binding to the free enzyme. The relatively weak binding of compound B to free *S. pneumoniae* PPAT was confirmed via isothermal titration calorimetry. In agreement with the kinetic studies, compound B was bound to *S. pneumoniae* PPAT in the absence of ATP. Analysis of binding thermograms produced significantly better fits to a model with two different classes of binding sites than to a model with only one class (see Fig. S2 in the supplemental material). Parameters determined for the first class of binding sites are  $K_d$  (dissociation constant) =  $0.27 \pm 0.05$   $\mu$ M, stoichiometry (per hexamer) =  $2.2 \pm 0.08$ , and  $\Delta H = -19.7 \pm 0.3$  kcal/mole; for the less potent class of binding sites,  $K_d = 6.3 \pm 0.9$   $\mu$ M, stoichiometry (per hexamer) =  $1.9 \pm 0.2$ , and  $\Delta H = -9.6 \pm 0.2$  kcal/mole.

**Cellular activity.** Increased potency of enzyme inhibition resulted in inhibition of growth for Gram-positive bacteria, with  $IC_{50}$ s of less than 20 nM needed to achieve measurable MICs ( $\leq 64$   $\mu$ g/ml), and continued optimization for enzyme inhibition ( $IC_{50}$ s < 1 nM) resulted in analogues that showed potent ( $\leq 8$   $\mu$ g/ml) MIC

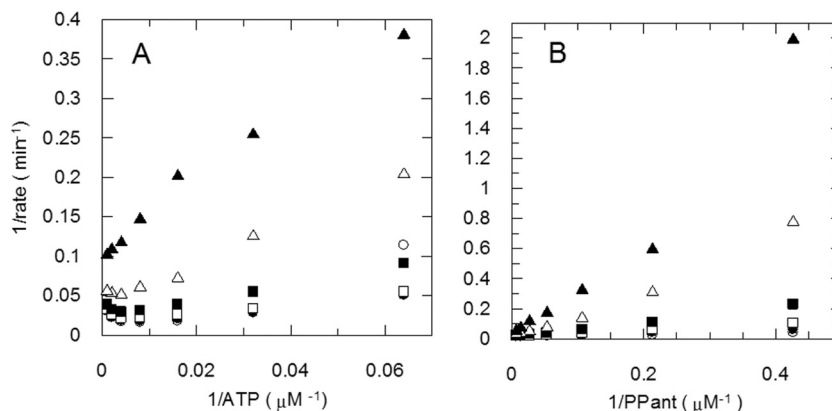


FIG 4 Reciprocal plot analysis of compound B inhibition of *S. aureus* PPAT. For clarity, plots are shown at only one concentration each for the paired substrates. The concentrations of inhibitor were 0  $\mu\text{M}$  (open circles), 0.1  $\mu\text{M}$  (filled circles), 0.3  $\mu\text{M}$  (open squares), 0.9  $\mu\text{M}$  (filled squares), 2.7  $\mu\text{M}$  (open triangles), and 8.1  $\mu\text{M}$  (filled triangles). Panel A shows the results obtained with 37.5  $\mu\text{M}$  4'-phosphopantetheine; panel B shows those obtained with 0.25 mM ATP.

values (Table 2). Such analogues were active ( $\text{MIC}_{90s} \leq 2 \mu\text{g/ml}$ ) against a variety of clinical Gram-positive isolates, including methicillin-resistant and quinolone-resistant *S. aureus*, macrolide-resistant *S. pneumoniae*, and vancomycin-resistant enterococci, as illustrated for compound D (Table 4). Despite the potent activity against Gram-positive species, no measurable inhibition of growth ( $\text{MIC} > 64 \mu\text{g/ml}$ ) of Gram-negative species was seen, even with efflux-compromised strains (Table 2). The compounds did not inhibit growth of yeast or of a mammalian cell line ( $\text{MIC} > 64 \mu\text{g/ml}$ ), with the exception of compound D, which showed some effect against a human cell line (Table 2).

To confirm that bacterial growth suppression was due to PPAT inhibition, mutants resistant to compound D were isolated, and the *coaD* gene of these mutants was sequenced. Resistant mutants could be generated for *S. aureus* and *S. pneumoniae* at frequencies of  $10^{-7}$  to  $10^{-9}$ , depending on the species and the selection concentration (Table 5), and the MICs of these mutants were elevated at least 8-fold (Table 6). Cross-resistance only to relevant project compounds and not to other chemical classes was seen (data not

shown). Sequencing of the *coaD* gene from these mutants showed mutations resulting in amino acid modifications in PPAT (Table 6), indicating that growth suppression in *S. aureus* and *S. pneumoniae* was due to inhibition of PPAT. This was confirmed for *S. pneumoniae* through genetic transformation of a PCR product containing altered *coaD* or chromosomal DNA from a *S. pneumoniae* *coaD*-resistant mutant into a susceptible strain, which resulted in transformants with mutated PPAT and elevated MICs against the dimethoxypyrimidines (data not shown). In addition, relevant project compounds showed elevated MIC values with a PPAT-overexpressing *S. pneumoniae* construct, supporting the notion that growth suppression occurred through PPAT inhibition in this species (Table 2).

Compounds in this series were bacteriostatic, with almost no reduction in culture viability for *S. aureus*, even after 24 h of compound exposure (Fig. 6). Although sterilization was achieved for *S. pneumoniae* in the killing kinetics experiment, the rate of killing was not accelerated compared to the rate seen with an untreated culture (Fig. 6). For both species, the compounds showed a delay

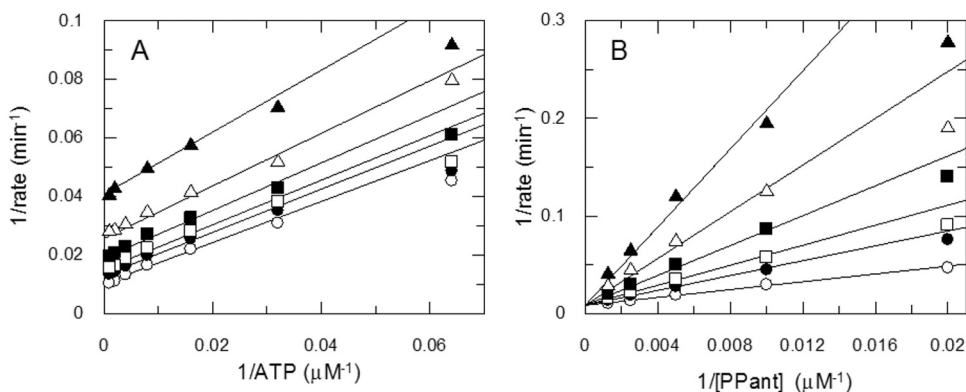


FIG 5 Mode-of-inhibition studies with compound B and *S. pneumoniae* PPAT. The dominant inhibition modality of compound B with *S. pneumoniae* PPAT is uncompetitive with ATP and competitive with 4'-phosphopantetheine. Lines indicate the best fit of data to equation 1. (A) Double reciprocal plot of 1/velocity versus 1/[ATP]. In the plot, only data for 800  $\mu\text{M}$  4'-phosphopantetheine are shown. The ATP concentration ranged from 15 to 1,000  $\mu\text{M}$ , with concentrations of inhibitor fixed at 0 nM (open circles), 15 nM (filled circles), 26 nM (open squares), 47 nM (filled squares), 83 nM (open triangles), and 150 nM (filled triangles). (B) Double reciprocal plot of 1/velocity versus 1/[PPant]. Data for 1,000  $\mu\text{M}$  ATP are shown. The 4'-phosphopantetheine concentration was adjusted from 50 to 800  $\mu\text{M}$ , and inhibitor concentrations were fixed as described for panel A. The data were fitted by the nonlinear least-squares method to a sequential kinetic mechanism, with inhibitor binding to both enzyme and enzyme-ATP complex. Initial velocity data were calculated as nM pyrophosphate produced  $\text{min}^{-1}$  per nM of enzyme monomer  $\text{min}^{-1}$ .

TABLE 3 Summary of mechanism-of-inhibition parameters for compound B with *S. pneumoniae* PPAT

Parameter <sup>a</sup>	Fitted value <sup>b</sup>
$k_{cat}$ (min <sup>-1</sup> )	125 ± 2
$K_{ia}$ (μM)	121 ± 9
$K_{ma}$ (μM)	54 ± 4
$K_{mb}$ (μM)	223 ± 9
$K_{i1}$ (μM)	0.29 ± 0.05
$K_{i2}$ (μM)	0.0122 ± 0.0004

<sup>a</sup> Substrate A (*ma*), ATP; substrate B (*mb*), 4'-phosphopantetheine.

<sup>b</sup> Error data represent standard errors based on the fit of data to equation 1.

<sup>c</sup> Determined as  $V_{max}/E_{tot}$ , with  $E_{tot}$  being the enzyme monomer concentration (3 nM).

in the onset of growth inhibition (growth continued upon initial exposure to compound; Fig. 6), which probably reflects the time required for depletion of an existing coenzyme A pool.

**Efficacy in mouse infection models.** Compounds C and D were tested in an immunocompetent mouse lung *S. pneumoniae* infection model. Mice were pretreated with ABT to reduce hepatic

TABLE 5 Spontaneous resistance frequencies for compound D for *S. pneumoniae* and *S. aureus*

Organism	Selection condition	Frequency of resistance
<i>S. pneumoniae</i>	1 × MIC	2.6E-7
	2 × MIC	3.7E-9
	4 × MIC	<3.1E-10
<i>S. aureus</i>	1 × MIC	1.8E-9
	2 × MIC	2.7E-9
	4 × MIC	7.7E-10

metabolism of the compounds in order to maximize exposure (33). While this pretreatment had limited effect on the clearance of compound C, clearance of compound D was reduced 6-fold from 64 to 11 ml/min/kg of body weight, indicative of P450 metabolism for this compound. For both compounds, dosing at 100 mg/kg four times a day resulted in stasis compared to the start of treatment (Fig. 7). PK analysis of these doses showed that the free

TABLE 4 Activity of compound D against Gram-positive clinical isolates<sup>a</sup>

Organism and parameter	Value(s)					
	Compound D	Linezolid	Erythromycin	Levofloxacin	Ceftriaxone	Vancomycin
<i>S. pneumoniae</i> (n = 70)						
MIC <sub>50</sub> (μg/ml)	0.004	1	0.125	1	ND	ND
MIC <sub>90</sub> (μg/ml)	0.008	1	>16	1	ND	ND
MIC range (μg/ml)	≤0.001 to 0.016	0.5 to 2	0.031 to >16	0.5 to 16	ND	ND
<i>S. pyogenes</i> (n = 69)						
MIC <sub>50</sub> (μg/ml)	0.125	2	ND	0.5	≤0.063	ND
MIC <sub>90</sub> (μg/ml)	0.5	2	ND	1	≤0.063	ND
MIC range (μg/ml)	0.031 to 1	1 to 32	ND	0.25 to 2	≤0.063 to ≤0.063	ND
<i>S. aureus</i> (n = 105)						
MIC <sub>50</sub> (μg/ml)	0.031	2	ND	0.25	8	ND
MIC <sub>90</sub> (μg/ml)	0.062	4	ND	>8	>64	ND
MIC range (μg/ml)	0.016 to 0.125	1 to 4	ND	0.0625 to >8	1 to >64	ND
MRSA (n = 25)						
MIC <sub>50</sub> (μg/ml)	0.062	2	ND	>8	>64	ND
MIC <sub>90</sub> (μg/ml)	0.125	4	ND	>8	>64	ND
MIC range (μg/ml)	0.016 to 0.025	1 to 4	ND	4 to >8	>64 to >64	ND
Enterococci (n = 32)						
MIC <sub>50</sub> (μg/ml)	1	2	ND	16	ND	2
MIC <sub>90</sub> (μg/ml)	2	8	ND	>16	ND	>32
MIC range (μg/ml)	0.125 to 4	1 to >16	ND	1 to >16	ND	0.5 to >32
<i>E. faecalis</i> (n = 16)						
MIC <sub>50</sub> (μg/ml)	0.5	2	ND	1	ND	2
MIC <sub>90</sub> (μg/ml)	1	2	ND	>16	ND	>32
MIC range (μg/ml)	0.125 to 1	2 to 2	ND	1 to >16	ND	0.5 to >32
<i>E. faecium</i> (n = 16)						
MIC <sub>50</sub> (μg/ml)	1	2	ND	>16	ND	>32
MIC <sub>90</sub> (μg/ml)	2	8	ND	>16	ND	>32
MIC range (μg/ml)	0.5 to 4	1 to >16	ND	1 to >16	ND	0.5 to >32
Other species						
<i>S. agalactiae</i> MIC (μg/ml)	4	ND	ND	2	ND	16
<i>S. milleri</i> MIC (μg/ml)	2	ND	ND	1	ND	16
<i>S. mitis</i> MIC (μg/ml)	≤0.016	ND	ND	2	ND	8
<i>S. mutans</i> MIC (μg/ml)	0.25	ND	ND	1	ND	8
<i>S. salivarius</i> MIC (μg/ml)	0.25	ND	ND	2	ND	8
<i>S. sanguis</i> MIC (μg/ml)	≤0.016	ND	ND	2	ND	8
<i>S. epidermis</i> MIC (μg/ml)	≤0.016	ND	ND	0.5	ND	8
<i>S. saprophyticus</i> MIC (μg/ml)	0.25	ND	ND	0.5	ND	32

<sup>a</sup> MRSA, methicillin-resistant *S. aureus*; ND, not determined.

TABLE 6 Characterization of compound D-resistant mutants of *S. aureus* and *S. pneumoniae*

Organism	Selection condition	Compound D MIC ( $\mu\text{g/ml}$ )	PPAT mutation
<i>S. pneumoniae</i> wild type	NA <sup>a</sup>	0.031	NA
<i>S. pneumoniae</i> mutant 1	2 $\times$ MIC	1	N107H
<i>S. pneumoniae</i> mutant 2	2 $\times$ MIC	0.125	F8L
<i>S. pneumoniae</i> mutant 3	2 $\times$ MIC	0.5	T117N
<i>S. aureus</i> wild type	NA	0.06	NA
<i>S. aureus</i> mutant 1	2 $\times$ MIC	4	N106H
<i>S. aureus</i> mutant 2	2 $\times$ MIC	4	N106Y
<i>S. aureus</i> mutant 3	2 $\times$ MIC	1	V136F

<sup>a</sup>NA, not applicable.

plasma concentrations of the compounds were above the MICs for at least half the duration of the experiment (see Fig. S3 in the supplemental material). A weaker response was observed in the mouse thigh *S. aureus* infection model. In that model, the same dose of compound C did not provide stasis compared to the start of treatment but a reduction of the bacterial burden of only about 1 log compared to the untreated control results (Fig. 7). Dosing at higher concentrations could not be attempted due to lack of solubility (compound D) or adverse effects (compound C).

**Drug-like properties of compounds.** Whereas activity of the molecules could be optimized, despite numerous efforts, other important compound properties, such as low protein binding, high solubility, sufficient *in vivo* stability, and low toxicity, could not be reconciled favorably with good biological activity. For example, compounds C and D both showed potent MIC values, but while compound C was highly soluble, it was rapidly cleared, and while compound D was improved in clearance, its solubility was low and signs of toxicity became apparent through weak activity against a mammalian cell line (Table 2). The potency against the mammalian cell line may be masked by the relatively high protein binding of the analogues (90% to 95%, depending on the species; Table 2), since mammalian cytotoxicity is measured in the presence of protein. Protein binding appears to affect the potency of the compounds, as the drug MIC for *S. aureus* measured in the presence of 50% human serum increased 16-fold.

## DISCUSSION

This report describes efforts to identify novel antibacterials acting through inhibition of PPAT, an essential enzyme in CoA biosyn-

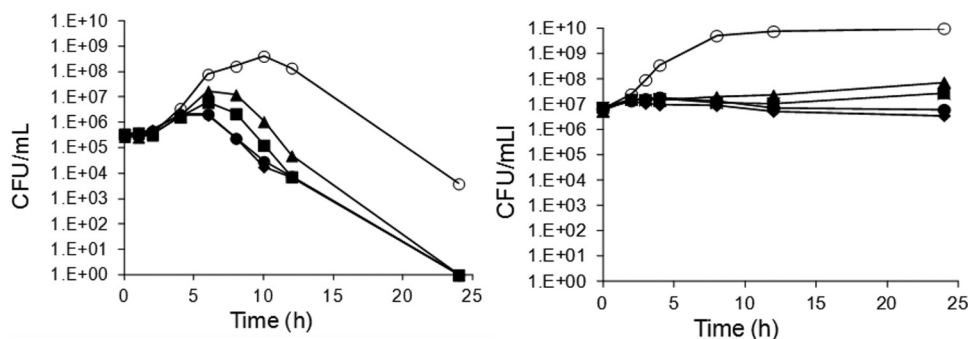


FIG 6 Killing kinetics for compound D with *S. pneumoniae* (left) and *S. aureus* (right). Cells were exposed to 0 $\times$  (open circles), 1 $\times$  (filled triangles), 2 $\times$  (filled squares), 4 $\times$  (filled circles), and 8 $\times$  (filled diamonds) the MIC, and killing of cells was measured by plotting CFU/ml over time. Compound D was added at 0 h.

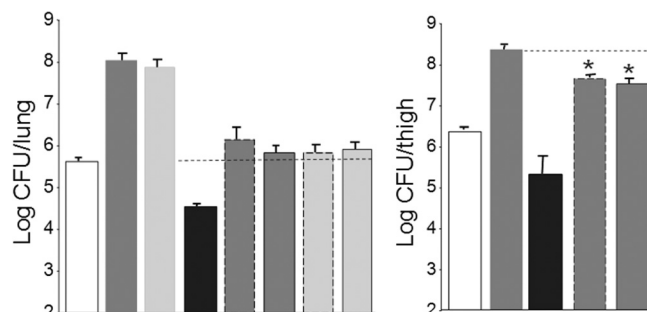


FIG 7 Efficacy in mouse *S. pneumoniae* lung infection model (left) for compounds C (dark gray bars) and D (light gray bars) and in mouse *S. aureus* thigh infection model (right) for compound C. Mice were treated at 100 mg/kg of body weight b.i.d. q4h (dashed outlines) or q.i.d. q4h (solid outlines). Data from pretreatment (white bars), vehicle growth controls for compounds C and D (no outline), and positive controls (black bars; see Materials and Methods) are included for comparison. The horizontal black dashed line indicates the level of stasis (left) or level of vehicle growth control (right). \*,  $P < 0.05$  compared to vehicle growth control (Mann-Whitney test).

thesis. Whereas inhibitors of this enzyme were identified previously (10, 11), none of these showed activity at the cellular level. The series of PPAT inhibitors described in this report represent the first reported set of compounds that not only inhibit the enzyme but, as a result, also suppress bacterial growth *in vitro* and affect bacterial burden in animal models, validating PPAT as a legitimate target for therapy against Gram-positive bacteria. These inhibitors were discovered through high-throughput screening with the isolated enzyme followed by optimization through medicinal chemistry efforts guided by X-ray crystallography. Although this approach may not always yield success (7, 8), this study provides another example of the ability of target-based screening to identify novel antibacterial agents. Unfortunately, while the activities led to a series with desirable activity, further progress into clinical development was hampered by the inability to reconcile this with favorable pharmacokinetics, high solubility, and low protein binding and/or low toxicity, as well as the potential for resistance development that is often encountered with agents directed against single gene targets (7).

**Biochemical characterization of PPAT inhibitors.** Kinetic and isothermal titration calorimetry studies with *S. pneumoniae* PPAT were in agreement, showing compound B of the cycloalkyl pyrimidine series to be competitive with 4'-phosphopantetheine and cobinding with ATP in an uncompetitive manner, in addition to a

second weaker mode of inhibition with the compound binding to free enzyme. Analysis of kinetic data for the *S. aureus* enzyme showed similarities to *S. pneumoniae* PPAT, with an inhibition modality for compound B competitive with 4'-phosphopantetheine but with a mixed-type inhibition profile with respect to ATP.

The results from the kinetic and isothermal titration calorimetric experiments were supported by analyses of cocrystal structures, which showed that the compounds bind to the 4'-phosphopantetheine pocket, with an accompanying ATP molecule present. While the most thorough kinetic studies were done with the *S. pneumoniae* enzyme and crystallography studies succeeded with the *S. aureus* enzyme, the high degree of PPAT sequence homology between these isozymes (see Fig. S4 in the supplemental material) reduces concerns that general findings for one species cannot be translated to others.

The cycloalkyl pyrimidines represent a new class of PPAT inhibitors, with activity against multiple bacterial PPAT isozymes. The compounds did not inhibit human PPAT enzyme, thereby showing desired antibacterial drug selectivity. Although members of this scaffold were more potent inhibitors of Gram-positive PPAT enzymes, they also had submicromolar  $IC_{50}$ s against PPAT of Gram-negative species (Table 2). Earlier studies reported on other 4'-phosphopantetheine-competitive PPAT inhibitors. Di-peptide-based inhibitors were designed to act as 4'-phosphopantetheine mimics, and crystallographic studies confirmed them to be bound in the 4'-phosphopantetheine site (11). This series was optimized for inhibition of *E. coli* PPAT, and the most potent compound in that series (compound 8) had a 6 nM  $IC_{50}$  but all lacked activity against bacteria. Pyrazoloquinolones (10) were identified by screening with *E. coli* PPAT and were characterized as ATP-competitive inhibitors. Although balanced activity against *E. coli* and *E. faecalis* PPAT was achieved, these compounds showed relatively low potency only, with  $K_i$  values at the single-digit micromolar level.

**Activity of PPAT inhibitors against bacteria.** Cycloalkyl pyrimidines represent the first reported series of compounds to show suppression of bacterial growth through inhibition of PPAT. The mode of action of the compound series was unequivocally established through genetic means, by generation of resistant mutants that were shown to have mutations in *coaD*, and by showing reduced susceptibility for a PPAT-overexpressing construct (Table 2). To achieve growth inhibition, very potent enzyme inhibition ( $IC_{50}$ s < 20 nM) was required. The reason for the high biochemical potency requirement is unclear, but it may have been due to poor compound penetration into the cell and/or may have been the result of a requirement to inhibit this enzyme to a high extent in order to achieve growth suppression, similar to the mechanism proposed for inhibitors of DNA ligase (41). It would be highly beneficial for a bacterium to express excess biosynthetic capacity for CoA, a cofactor that plays a central role in many cellular processes, to absorb minor disturbances in biosynthesis without disrupting growth.

The compounds showed a spectrum of activity limited to Gram-positive species. As expected for compounds with a novel mode of action, cycloalkyl pyrimidines were equally active against strains susceptible to and strains resistant to clinically approved drugs (Table 4). The lack of growth inhibition for Gram-negative species was probably due to lower potency for inhibition of Gram-negative PPAT enzymes (Table 2), combined with poor com-

ound penetration. Compound penetration into Gram-negatives is a general issue for many compounds (42).

The compounds did not accelerate killing kinetics for *S. aureus* or *S. pneumoniae* compared to the results for untreated cultures that reached stationary phase. In addition, onset of growth suppression was delayed, most likely due to the time required for depletion of an existing CoA pool (14). These findings are similar to those from another class of cofactor biosynthesis inhibitors, the sulfonamides, which inhibit dihydropteroate synthetase, an enzyme involved in biosynthesis of the cofactor folate (43). It can be anticipated that inhibitors of biosynthesis of other cofactors, such as riboflavin and biotin, may show similar microbiological properties. Although a delay in the onset of growth inhibition and slow killing kinetics might be expected to negatively impact the efficacy of treatment, compounds with such properties have been successfully used in the clinic, as evidenced by the sulfonamides. Furthermore, the consensus is that there is no evidence supporting use of cidal over static drugs for bacterial diseases aside from endocarditis and meningitis (44).

Resistant mutants could be isolated with high frequency but only at concentrations of compound of less than 4-fold the MIC (Table 5). The drug MIC values for the mutants were significantly elevated for PPAT inhibitors due to target modifications (Table 6), and coverage of such mutants would require significant higher compound exposures. Moreover, at least for *S. aureus*, inhibition of PPAT is not a rapidly cidal event and allows selection of resistant mutants when compound exposure drops below therapeutic levels. However, the reduced isolation of spontaneous resistant mutants at elevated compound concentrations, and the fact that no resistant mutants emerged during killing kinetics experiments, even upon prolonged incubation, may indicate a low mutant prevention concentration (MPC) (45) for these compounds. Thus, the disadvantage of PPAT as a target with poor cidal activity that allows for selection of mutants with significantly elevated drug MIC values may be offset by a low MPC. Further experimentation, using multiple strains, would be required to test this hypothesis.

**Efficacy in animal models.** The lead compounds in the series showed an effect on bacterial burden in two animal models, with stasis achieved in the *S. pneumoniae* lung model (Fig. 7). Higher doses and/or prolonged duration of dosing, to take into consideration the observed delayed onset of growth inhibition and poor killing kinetics seen *in vitro*, would likely lead to an improved response. However, these could not be attempted with the current compounds due to poor solubility and lack of tolerability. In the *S. aureus* thigh model, even stasis was not achieved at the same doses, but given the even slower killing kinetics observed *in vitro* with this species compared to *S. pneumoniae*, this outcome could have been expected. Alternatively, poor compound penetration into thigh, and/or higher CoA pool levels in *S. aureus*, may have contributed to the poorer response in this model.

**In conclusion.** A series of cycloalkyl pyrimidines was identified through high-throughput screening and optimized through a medicinal chemistry program guided by crystallography. The lead compounds of the series suppressed growth of Gram-positive bacteria through inhibition of PPAT and demonstrated effects on bacterial burden in two mouse efficacy models, thereby validating PPAT as a novel target for antibacterial therapy. Reconciling these favorable biological properties with other properties needed for drugs appeared not to be possible, preventing progression of this series into clinical development. Additional efforts will be re-

quired to identify PPAT inhibitors that can progress into the clinic, hopefully leading to other potent compounds with low resistance potential that can be used in treatment of infections for which current therapies have become limited as a result of resistance development.

## ACKNOWLEDGMENTS

We thank members of the microbiology susceptibility testing, pharmacology, and DMPK groups for performing MIC determinations, executing efficacy studies, and physical chemical measurements on the compounds, respectively, and Kathy MacCormack for DNA sequencing.

## REFERENCES

- Fauci AS, Morens DM. 2012. The perpetual challenge of infectious diseases. *N. Engl. J. Med.* 366:454–461.
- Roberts RR, Hota B, Ahmad I, Scott RD, Foster SD, Abbasi F, Schabowski S, Kampe LM, Ciavarella GG, Supino M, Naples J, Cordell R, Levy SB, Weinstein RA. 2009. Hospital and societal costs of antimicrobial-resistant infections in a Chicago teaching hospital: implications for antibiotic stewardship. *Clin. Infect. Dis.* 49:1175–1184.
- Arias CA, Murray BE. 2009. Antibiotic-resistant bugs in the 21st century—a clinical super-challenge. *N. Engl. J. Med.* 360:439–443.
- Nordmann P, Poirel L, Toleman MA, Walsh TR. 2011. Does broad-spectrum  $\beta$ -lactam resistance due to NDM-1 herald the end of the antibiotic era for treatment of infections caused by Gram-negative bacteria? *J. Antimicrob. Chemother.* 66:689–692.
- Bush K, Courvalin P, Dantas G, Davies J, Eisenstein B, Huovinen P, Jacoby GA, Kishony R, Kreiswirth BN, Kutter E, Lerner SA, Levy S, Lewis K, Lomovskaya O, Miller JH, Mobashery S, Piddock LJV, Projan S, Thomas CM, Tomasz A, Tulkens PM, Walsh TR, Watson JD, Witkowski J, Witte W, Wright G, Yeh P, Zgurskaya HI. 2011. Tackling antibiotic resistance. *Nat. Rev. Microbiol.* 9:894–896.
- Levy SB, Marshall B. 2004. Antibacterial resistance worldwide: causes, challenges and responses. *Nat. Med.* 10:S122–S129.
- Silver LL. 2011. Challenges of antibacterial discovery. *Clin. Microbiol. Rev.* 24:71–109.
- Payne DJ, Gwynn MN, Holmes DJ, Pompliano D. 2007. Drugs for bad bugs: confronting the challenges of antibacterial discovery. *Nat. Rev. Drug Discov.* 6:29–40.
- Barrett JF. 2006. Impact of genomics—emerging targets for antibacterial therapy. *Comp. Med. Chem. II* 7:731–748.
- Miller JR, Thanabal V, Melnick MM, Lall M, Donovan C, Sarver RW, Lee D-Y, Ohren J, Emerson D. 2010. The use of biochemical and biophysical tools for triage of high-throughput screening hits—a case study with *Escherichia coli* phosphopantetheine adenylyltransferase. *Chem. Biol. Drug Des.* 75:444–454.
- Zhao L, Allanson NM, Thomson SP, Maclean JFK, Barker JJ, Primrose WU, Tyler PD, Lewendon A. 2003. Inhibitors of phosphopantetheine adenylyltransferase. *Eur. J. Med. Chem.* 38:345–349.
- Zhang YM, White SW, Rock CO. 2006. Inhibiting bacterial fatty acid synthesis. *J. Biol. Chem.* 281:17541–17544.
- Spry C, Kirk K, Saliba KJ. 2008. Coenzyme A biosynthesis: an antimicrobial drug target. *FEMS Microbiol. Rev.* 32:56–106.
- Leonardi R, Zhang Y-M, Rock CO, Jackowski S. 2005. Coenzyme A: back in action. *Progr. Lipid Res.* 44:125–153.
- Izard T, Geerlof A. 1999. The crystal structure of a novel bacterial adenylyltransferase reveals half of sites reactivity. *EMBO J.* 18:2021–2030.
- Geerlof A, Lewendon A, Shaw WV. 1999. Purification and characterization of phosphopantetheine adenylyltransferase from *Escherichia coli*. *J. Biol. Chem.* 274:27105–27111.
- Freiberg C, Wieland B, Spaltmann F, Ehlert K, Brötz H, Labischinski H. 2001. Identification of novel essential *Escherichia coli* genes conserved among pathogenic bacteria. *J. Mol. Microbiol. Biotechnol.* 3:483–489.
- Gerdes SY, Scholle MD, D'Souza M, Bernal A, Bae MV, Farrell M, Kurnasov OV, Daugherty MD, Mseeh F, Polanuyer BM, Campbell JW, Anantha S, Shatalin KY, Chowdhury SAK, Fonstein MY, Osterman AL. 2002. From genetic footprinting to antimicrobial drug targets: examples in cofactor biosynthetic pathways. *J. Bacteriol.* 184:4555–4572.
- Daugherty M, Polanuyer B, Farrell M, Scholle M, Lykidis A, de Crecy-Lagard V, Osterman A. 2002. Complete reconstitution of the human coenzyme A biosynthetic pathway via comparative genomics. *J. Biol. Chem.* 277:21431–21439.
- Genschel U. 2004. Coenzyme A biosynthesis: reconstruction of the pathway in archaea and an evolutionary scenario based on comparative genomics. *Mol. Biol. Evol.* 21:1242–1251.
- Mandel AL, La Clair JJ, Burkart MD. 2004. Modular synthesis of pantetheine and phosphopantetheine. *Org. Lett.* 6:4801–4803.
- Mills SD, Eakin AE, Buurman ET, Newman JV, Gao N, Huynh H, Johnson KD, Lahiri S, Shapiro AB, Walkup GK, Yang W, Stokes SS. 2011. Novel bacterial NAD<sup>+</sup>-dependent DNA ligase inhibitors with broad-spectrum activity and antibacterial efficacy in vivo. *Antimicrob. Agents Chemother.* 55:1088–1096.
- Clinical and Laboratory Standards Institute. 2009. Methods for dilution antimicrobial susceptibility tests for bacteria that grow aerobically; approved standard, 9th ed. M07-A8, vol 29, no. 2. Clinical and Laboratory Standards Institute, Wayne, PA.
- National Committee for Clinical Laboratory Standards. 1999. Methods for determining bactericidal activity of antimicrobial agents; approved guideline. M26-A, vol 19, no. 18. National Committee for Clinical Laboratory Standards, Wayne, PA.
- Tomasz A, Moreillon P, Pozzi G. 1988. Insertional inactivation of the major autolysin gene of *Streptococcus pneumoniae*. *J. Bacteriol.* 170:5931–5934.
- Yang J, Copeland RA, Lai Z. 2009. Defining balanced conditions for inhibitor screening assays that target bisubstrate enzymes. *J. Biomol. Screen.* 14:111–120.
- Shapiro AB, Gao N, Thresher J, Walkup GK, Whiteaker J. 2011. A high-throughput absorbance-based assay for methionine produced by methionine aminopeptidase using S-adenosyl-L-methionine synthetase. *J. Biomol. Screen.* 16:494–505.
- Keating TA, Newman JV, Olivier NB, Otterson LG, Andrews B, Boriack-Sjodin PA, Breen JN, Doig P, Dumas J, Gangl E, Green OM, Guler SY, Hentemann MF, Joseph-McCarthy D, Kawatkar S, Kutschke A, Loch JT, McKenzie AR, Pradeepan S, Prasad S, Martínez-Botella G. 2012. *In vivo* validation of thymidylate kinase (TMK) with a rationally-designed, selective antibacterial compound. *ACS Chem. Biol.* 7:1866–1872.
- Jancarik J, Kim SH. 1991. Sparse matrix sampling: a screening method for crystallization of proteins. *J. Appl. Crystallogr.* 24:409–411.
- Smart OS, Womack TO, Flensburg K, Keller P, Pacionek W, Sharff A, Vonnrhein C, Bricogne G. 2012. Exploiting structure similarity in refinement: automated NCS and target-structure restraints in BUSTER. *Acta Crystallogr. D Biol. Crystallogr.* 68(Pt 4):368–380.
- Emsley P, Cowtan K. 2004. Coot: model-building tools for molecular graphics. *Acta Crystallogr. D Biol. Crystallogr.* 60(Pt 12 Pt 1):2126–2132.
- Laskowski RA, MacArthur MW, Moss DS, Thornton JM. 1993. PROCHECK—a program to check the stereochemical quality of protein structures. *J. Appl. Cryst.* 26:283–291.
- Balani SK, Li P, Nguyen J, Cardoza K, Zeng H, Mu D-X, Wu J-T, Gan L-S, Lee FW. 2004. Effective dosing regimen of 1-aminobenzotriazole for inhibition of antipyrine clearance in guinea pigs and mice using serial sampling. *Drug Metab. Dispos.* 32:1092–1095.
- Azoulay-Dupuis E, Bedos JP, Vallée E, Hardy DJ, Swanson RN, Pocardo JJ. 1991. Antipneumococcal activity of ciprofloxacin, ofloxacin, and temafloxacin in an experimental mouse pneumonia model at various stages of the disease. *J. Infect. Dis.* 163:319–324.
- Sherer BA, Hull K, Green O, Basarab G, Hauck S, Hill P, Loch JT, Mullen G, Bist S, Bryant J, Boriack-Sjodin A, Read J, DeGrace N, Uria-Nickelsen M, Illingworth RN, Eakin AE. 2011. Pyrrolamide DNA gyrase inhibitors: optimization of antibacterial activity and efficacy. *Bioorg. Med. Chem. Lett.* 21:7416–7420.
- Yoon HJ, Kang JY, Mikami B, Lee HH, Suh SW. 2011. Crystal structure of phosphopantetheine adenylyltransferase from *Enterococcus faecalis* in the ligand-unbound state and in complex with ATP and pantetheine. *Mol. Cells* 32:431–435.
- Leskovac V. 2003. Comprehensive enzyme kinetics. Kluwer Academic Press, Boston, MA.
- Izard T. 2002. The crystal structures of phosphopantetheine adenylyltransferase with bound substrates reveal the enzyme's catalytic mechanism. *J. Mol. Biol.* 315:487–495.
- Miller JR, Ohren J, Sarver RW, Mueller WT, de Dreu P, Case H, Thanabal V. 2007. Phosphopantetheine adenylyltransferase from *Escherichia coli*: investigation of the kinetic mechanism and role in regulation of coenzyme A biosynthesis. *J. Bacteriol.* 189:8196–8205.

40. Segel IH. 1975. Enzyme kinetics. Wiley-Interscience, New York, NY.
41. Korycka-Machala M, Rychta E, Brzostek A, Sayer HR, Rumijowska-Galewicz A, Bowater RP, Dziadek J. 2007. Evaluation of NAD<sup>+</sup>-dependent DNA ligase of mycobacteria as a potential target for antibiotics. *Antimicrob. Agents Chemother.* 51:2888–2897.
42. Kumar A, Schweizer HP. 2005. Bacterial resistance to antibiotics: active efflux and reduced uptake. *Adv. Drug Deliv. Rev.* 57:1486–1513.
43. Seydel JK, Wempe E, Miller GH, Miller L. 1973. Quantification of the antibacterial action of trimethoprim alone and in combination with sulfonamides by bacterial growth kinetics. *J. Infect. Dis.* 128(Suppl): 463–469.
44. Finberg RW, Moellering RC, Tally FP, Craig WA, Pankey GA, Dellinger EP, West MA, Joshi M, Linden PK, Rolston KV, Rotschafer JC, Rybak MJ. 2004. The importance of bactericidal drugs: future directions in infectious disease. *Clin. Infect. Dis.* 39:1314–1320.
45. Blondeau JM. 2009. New concepts in antimicrobial susceptibility testing: the mutant prevention concentration and mutant selection window approach. *Vet. Dermatol.* 20:383–396.